DE-SHADING: INTEGRATED APPROACH TO PHOTOMETRIC MODEL, SURFACE SHAPE AND REFLECTANCE PROPERTIES

Xiuguang Zhou, Egon Dorrer
Inst. f. Photo. u. Karto., Universität der Bundeswehr München, Germany

ISPRS Commission , Working Group WG III/2

KEY WORDS: Cartography, Surface, Understanding, Research, Experiment, Computer Vision, Photometric Model, Image De-shading System.

ABSTRACT:

A de-shading problem is presented in this paper. By using a brightness image and its associated height image, the de-shading problem is stated by estimating the approximate photometric model, the surface reflectance properties and an improved precision of the given height image. Proposed is a de-shading system. It contains a training frame and a working frame. In the training frame, a probing algorithm is proposed to determine the approximate photometric model amongst some candidate models. In the working frame, a region growing algorithm based on least square fitting is proposed to determine the inhomogeneous surface reflectance properties and a shape from shading algorithm is applied to improve the precision of the given height image. Synthetic images generated by using the Lambertian model and the Torrance-Sparrow model were used as test images in the experiments. The results are given to illustrate the usefulness of our approach.

1. INTRODUCTION

There are some common interesting topics in computer vision, remote sensing, photogrammetry, cartography and their relative communities, such as shaded-relief, surface reflectance properties, photometric model, the direction of the light source and shape from shading (SFS). As is well known, shaded-relief (shading) is to illuminate a surface by using a given light source or multiple light sources (Brassel, 1973; Horn, 1982; Zhou and Dorrer, 1995). The surface reflectance properties are important to study material properties. This is of interest in remote sensing for observing Earth and the planets. Recently, the surface reflectance properties have been determined by using the range and brightness data (Bibro and Snyder, 1988; Ikeuchi and Sato, 1991; Kay and Caelli, 1994). Shade recovery is a classic problem in computer vision. One of the techniques to recover shape is shape-from-shading, which deals with the recovery of shape from a gradual variation of shading in the image (Ikeuchi and Horn, 1981; Pentland, 1984; Brooks and Horn, 1985; Lee and Rosenfeld, 1985; Zheng and Cellappa, 1991; Kimmel and Bruckstein, 1995). There exists quite a number of photometric models, such as the widely used Lambertian model, the famous Torrance-Sparrow model (Torrance and sparrow, 1967) and the Phong model (Phong, 1975). These models are used to describe reflectance maps.

The so-called de-shading in this paper deals with the above topics. Briefly, de-shading is to remove the natural illumination from an image to obtain the original information of the object in the image. It is the inverse procedure of shading. As known, a shading procedure is to generate an illuminated image by using the given light source, photometric model, albedo or surface reflectance properties and the height image (digital terrain model, DTM). Inversely, if one has an image (maybe a remote sensing image) and its associated height image (maybe a DTM), the following questions might be interesting. What is the approximate photometric model of the image? Where is the light source for the image? What are the reflectance properties of the surface? How to increase the precision of the existing DTM if it is not accurate enough? De-shading tries to solve these problems.

De-shading is very useful in different application fields such as computer vision, remote sensing, photogrammetry and cartography, etc. In the area of remote sensing, e.g., as more and more DTMs are being successfully generated, one may want to use the DTM to study the surface properties of the Earth or other planets. Due to some inadequate conditions (e.g. inadequacy of matching algorithm, insufficient information in the shadow region or errors of the interpolation, etc.), the precision of the DTM may be insufficient. Therefore, to increase the precision of an existing DTM is of great important. Also, one may want to mosaic two remote sensing images with different directions of illumination. For this problem, we need first to remove the illuminations of both images (de-shading), then re-shade the de-shaded images with an assigned illumination direction based on the obtained proper photometric model, reflectance properties and improved precision of the DTM.

2. CONCEPTION AND DEFINITION

As is known, the visual brightness image is the signal recorded from one or more sensor(s). The sensor receives the visual light reflected from the surface of the object. The reflected light comes from the source light which strikes the surface. If the illumination of an image is removed, what will remain? Roughly, there will be nothing to be seen. Because no light source means no visual information. But if we consider the information recorded on an image, there should be something "hidden" under the illumination. The information of a visual image may contain: the direction and energy of the light source, the reflectance properties of the surface, the geometric information of the surface, the photometric model information, the atmospheric affecting information, the noise information and so on. Obviously, even if the illumination were taken out, some image information still exists. In other words, some of the information hidden in the visual grey values is possible to be estimated. Of course, it is very difficult to get some of the information listed above (may not be possible to obtain if there are not enough additional conditions). We named the process of obtaining some of the hiding image information as de-shading. In the following, the definition, the task and the inputs-outputs of the de-shading are given.

Definition of de-shading: Remove the natural expressive illumination from a visual image to obtain the original information of the object and the information in the imagery.

Task of de-shading: Given a real image and its associated approximate height image, the task of de-shading is to obtain the photometric model approximating the real image, the albedo or surface reflectance properties, the direction of the light source and the improved height image which has a higher precision than the approximate input height image.

Inputs and outputs: The inputs of a de-shading system are: some candidate photometric models, a brightness image and its associated approximate height image (range image or DTM image). The outputs are: the light source, the photometric model approximating the brightness image, the albedo image or the surface reflectance properties image (the value of each pixel in each image represents the albedo value or reflectance property value at its coordinates), the improved height image which is more precise than the approximate input height image.

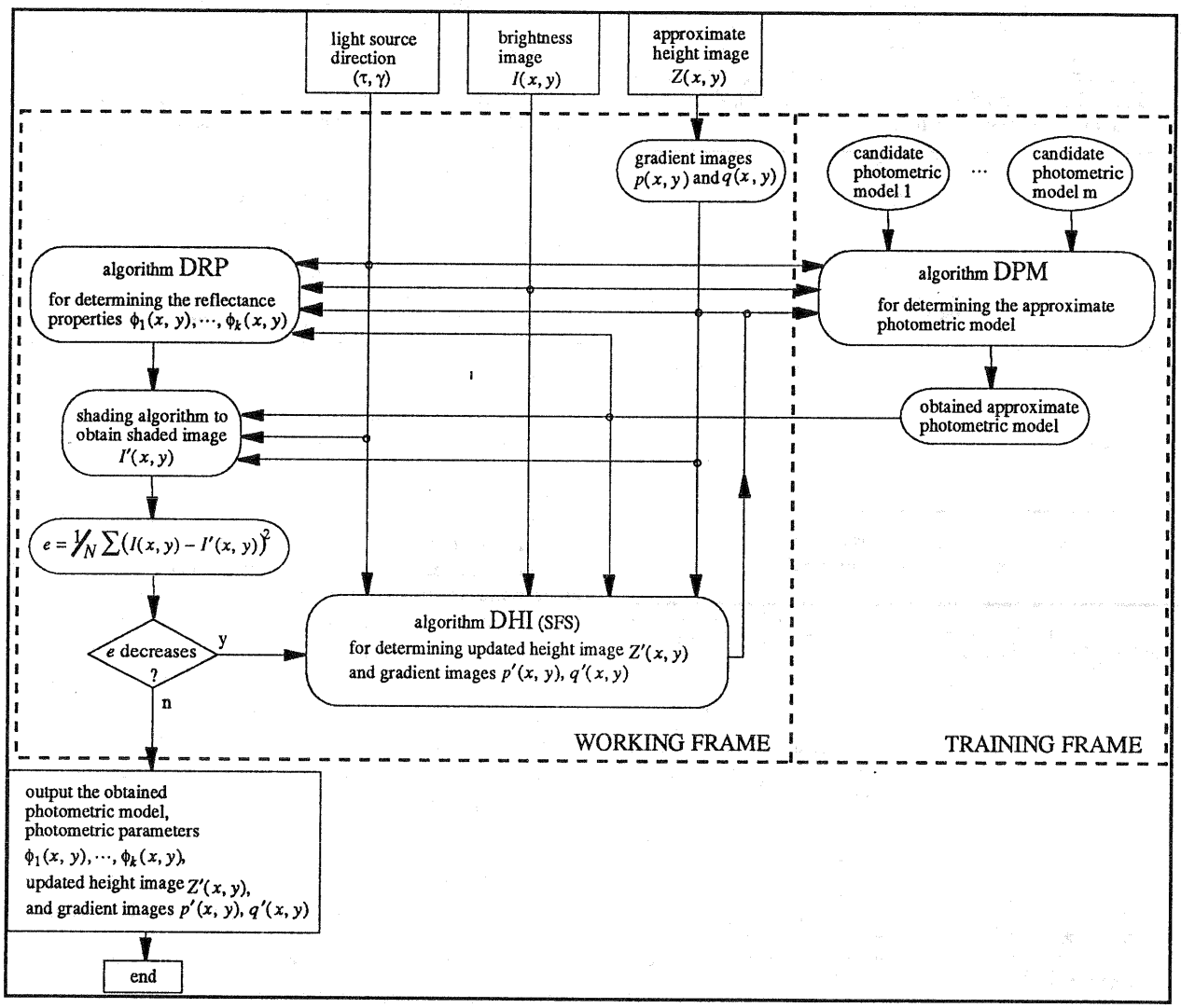

Fig.2. A de-shading system.

3. DE-SHADING SYSTEM

A de-shading system is proposed in the paper to perform the de-shading task. As described in the above section, the task of de-shading is to obtain the surface reflectance properties, the light source, the improved higher precision height image and the approximate photometric model from a given brightness image and its associated approximate height image. Obviously, this is not easy. Fortunately, there exist some methods being more or less relevant to parts of the task. E.g., the least square fitting method is used to calculate the surface reflectance properties (Ikeuchi and Sato, 1991; Kay and Caelli, 1994), SFS is used to obtain the surface orientation and height image (Ikeuchi and Horn, 1981; Pentland, 1984; Brooks and Horn, 1985; Lee and Rosenfeld, 1985; Zheng and Cellappa, 1991; Kimmel and Bruckstein, 1995). But all the methods need some strong preconditions. Algorithms for calculating surface reflectance properties assume that the photometric model is known and that the reflectance properties are homogeneous over the entire surface, also a precision range image is required. The SFS algorithms assume that the surface reflectance properties and the photometric model are known. Unfortunately, the assumptions might be wrong or the preconditions might not be available in practice. The photometric model plays an important role in these problems. In order to get the approximate photometric model, a probing method may be appropriate. It means, one can approximate the correct photometric model by using different known models as probing models. The proper model will yield the least error between the brightness image and the shaded image obtained by using the probing photometric model. But the precondition of this method needs a precision height image and the correct photometric parameters (reflectance properties). As we see so far, the difficulty is that one solution depends on another in a circular problem. If we divide the de-shading task into three sub-tasks: Determining Photometric Model (DPM), Determining Reflectance Properties (DRP) and Determining improved Height Image (DHI), each of these sub-tasks needs the outputs of the other two as its inputs. This can be illustrated as in Fig. 1.

Considering the above analysis, a de-shading system shown in Fig. 2 is developed to perform the de-shading problem. It contains two frames. One is the training frame, the other is the working frame. The inputs to this system are the illumination direction (τ, γ), a brightness image $I(x, y)$, and an

approximate height image (DTM for remote sensing). In order to simplify the system, we assume that the light source is known. This is true for most of the applications. For remote sensing area, we can get the illumination direction from the header of the image file. In close-range photogrammetry area, the illumination direction is also known, because the light source is assigned by the experimentater. If the illumination direction is unknown, one can calculate it by using Pentland's method (1982), Lee and Rosenfeld's method (1989), Zheng and Chellappa's method (1991) or others.

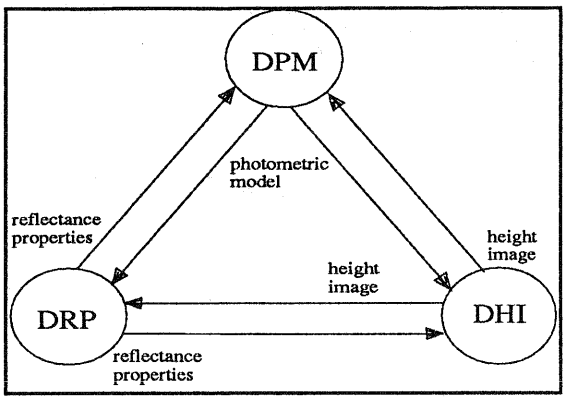

Fig. 1 Schematic of inputs and outputs among the three algorithms.

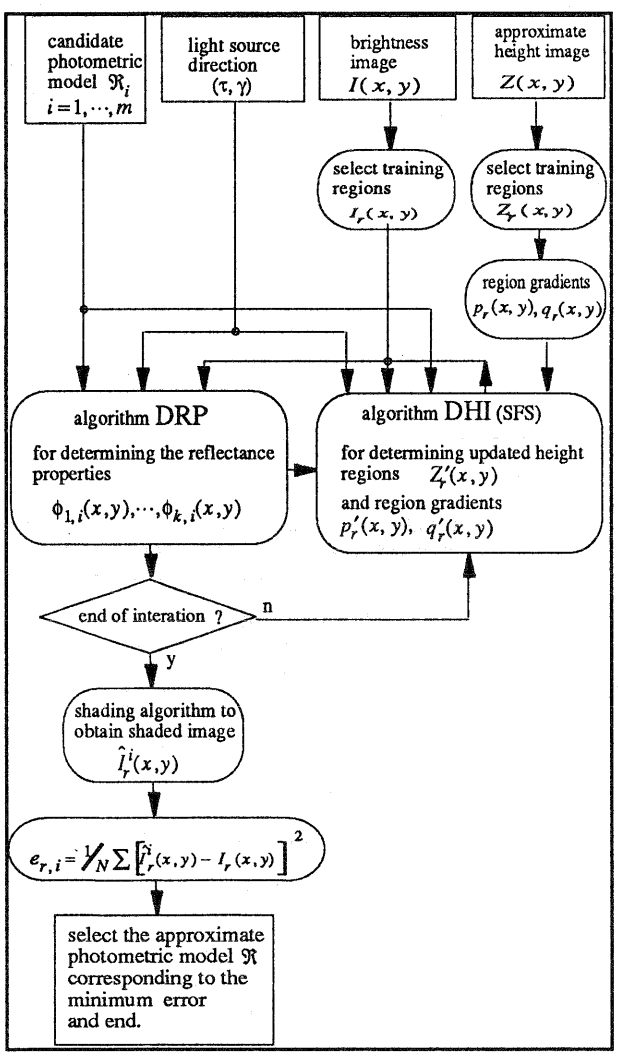

Fig. 3 Diagram of DPM algorithm.

3.1 Training Frame

The training frame contains one algorithm (DPM) for determining the approximate photometric model. Some small regions are selected as the training regions for determining the approximate photometric model. In our algorithm, five small regions are selected. One small region is located at the centre of the brightness image and the height image. The other four are located at the four centres of the upper-left, upper-right, lower-left and lower-right quarters of the brightness image and height image. Several photometric models are assigned as candidate models. All candidate models are tested in the training regions to find an approximate photometric model. For every candidate model, the algorithm (DRP) for determining reflectance properties (see the working frame) and the algorithm (DHI) for determining the updated improved height image (see the working frame) are combined to construct an iterative procedure to find the goodness of the approximation. A fixed number of iteration is used in the training frame. After the iterations, for every candidate photometric model, a set of reflectance properties (photometric parameters) with respect to every pixel in the training regions and the updated improved height data in the training regions are obtained. Using these reflectance properties and the improved height data, a shading algorithm is carried out to obtain the artificially shaded regions. A mean square error, corresponding to every candidate photometric function, between the shaded region and the original brightness regions are calculated. The candidate model corresponding to the minimum error is selected as the approximate photometric model. Let $\Re_i$ $i=1,\cdots,m$ be the i th model of m candidate photometric models. Let $\phi_{1,r}(x,y),\cdots,\phi_{k,r}(x,y)$ be the k photometric parameters of the i th candidate photometric model obtained from DRP after the iterations. Let $p_r'(x,y)$ and $q_r'(x,y)$ be the updated gradients in the training regions obtained from DHI after the iterations. The shaded regions $\hat{I}_r^i(x,y)$ is

$$\hat{I}_r^i(x,y)=\Re_i\left(p_r'(x,y),q_r'(x,y),\phi_{1,i}(x,y),\cdots,\phi_{k,i}(x,y)\right),$$

for candidate photometric model i. (1)

The mean square error $e_{r,i}$ between the shaded training regions and the brightness image in the training regions is

$$e_{r,i}=1/N\Sigma\left[\hat{I}_r^i(x,y)-I_r(x,y)\right]^2,$$

for candidate photometric model i. (2)

The determined approximate photometric model $\Re$ is thus given by

$$\Re=\Re_i\Big|\min_i\left\{e_{r,i}\right\} \quad (3)$$

The DPM algorithm is illustrated in Fig. 3. In fact, it is similar to the structure of the working frame in Fig. 2.

3.2 Working Frame

The working frame mainly contains two algorithms. The algorithm DRP is for determining the reflectance properties. The algorithm DHI is for determining the updated improved height image. We developed a region growing algorithm to determine the surface properties within DRP. In DHI, we follow Zheng and Chellappa's method (1991).

By using the photometric model $\Re$ determined in the training frame, the known light source, with the brightness image and the approximate height image, we first estimate the surface reflectance property images in DRP. The number of the reflectance property images depends on how many parameters are used in the determined photometric model. E.g., if it is the Torrance-Sparrow model, there are three reflectance property images (the diffusion parameter image, the specular parameter image and the surface roughness parameter image). The value of each pixel in the property image represents the value of surface reflectance property at its coordinates. If it is the Lambertian model there is only one image containing albedo values. Then these estimated reflectance properties are used in DHI to improve the approximate height image. The improved height image is then used to improve the estimation of the reflectance property image(s), and so on. Obviously, this is an iteration strategy. In each iteration, a shading algorithm is called to obtain the shaded image. The mean square error between the brightness image and the shaded image is calculated to determine whether the iteration should be stopped. If the mean square error does not reduce, the program terminates and outputs the determined photometric model, the surface reflectance property image(s) and the improved height image.

3.2.1 DRP - A Region Growing Algorithm to Determine Surface Reflectance Properties

So far, our problem becomes to obtain the surface reflectance properties based on a given photometric model, a given brightness image and a given height image. Though this seems similar with the problem in Ikeuchi and Sato's paper (1991) and the problem in Kay and Caelli's paper (1994), there are significant differences with their cases. We estimate parameters at each point on the object surface. Our method differs from that of Ikeuchi and Sato which assumed constant regions. Also, our method differs from that of Kay and Caelli which used multiple brightness images obtained with different light sources.

A region growing algorithm based on least square fitting is proposed to estimate the inhomogeneous reflectance properties. In the algorithm, a set of initial reflectance properties are estimated in a set of kernel surface points. Surface reflectance properties are obtained by minimizing

$$e_{\Omega_k} = \sum_{x,y \in \Omega_k} \left[I(x,y) - \hat{I}_{\Re}(x,y) \right]^2, \tag{4}$$

where Ω_k is the set of kernel points, I is the brightness image, $\hat{I}_{\Re}$ is the image irradiance corresponding to the photometric model $\Re$. For the Lambertian model, Eq. 4 becomes

$$e_{\Omega_k} = \sum_{x,y \in \Omega_k} \left[I(x,y) - c_d \cdot \mathbf{S} \cdot \mathbf{N}(x,y) \right]^2, \tag{5}$$

where c_d is the Lambertian diffuse reflection coefficient. S is the direction of light source, N is the surface normal. For the Torrance-Sparrow model, Eq. 4 becomes

$$e_{\Omega_k} = \sum_{x,y \in \Omega_k} \left[I(x,y) - c_d \cdot \mathbf{S} \cdot \mathbf{N}(x,y) - c_s \cdot \exp(-c_r^2 \cdot \alpha(x,y)^2) \right]^2, \tag{6}$$

where c_s is the specular coefficient, c_r is the surface roughness coefficient, α is the specular angle calculated as

$$\alpha(x,y) = \cos^{-1}(\mathbf{H} \cdot \mathbf{N}(x,y)), \tag{7}$$

where $\mathbf{H} = (\mathbf{S}+\mathbf{V}) / \|\mathbf{S}+\mathbf{V}\|$ with V the viewing direction.

The minimization of Eq. 5 to obtain c_d is simple. To minimize Eq. 6 to obtain c_d, c_s and c_r, we follow Kay and Caelli's method. From the kernel set, we grow the neighbours of the kernel set if the neighbours have the same properties as the kernel set. Whether a neighbour point is to be grown depends on the error after growing. Let $\Omega_k + 1$ denote the new set of the kernel set Ω_k adding a neighbour point. Let c_{d,Ω_k}, c_{s,Ω_k} and c_{r,Ω_k} be three parameters estimated in set Ω_k. The error e_{Ω_k+1} is

$$e_{\Omega_k+1} = \sum_{x,y \in \Omega_k+1} [I(x,y) - c_{d,\Omega_k} \cdot \mathbf{S} \cdot \mathbf{N}(x,y) - c_{s,\Omega_k} \cdot \exp(-c_{r,\Omega_k}^2 \cdot \alpha(x,y)^2)]^2. \tag{8}$$

If

$$\left| e_{\Omega_k+1} \right| < th, \tag{9}$$

this neighbour point is added to the kernel set. In Eq. 9, th is a predefined threshold. Therefore, the new kernel set has one point more. After the neighbours of the old kernel set Ω_k are tested and the kernel set has grown, parameters c_d, c_s and c_r are re-estimated and updated. If the kernel set has not grown, the growing for set Ω_k is stopped. The growing will start with a new kernel set until all points on the surface are estimated. The initial kernel set can be a small $n \times n$ window anywhere. However, the deviation of $\left[I(x,y) - \hat{I}_{\Re}(x,y) \right]^2$ must be small by using the estimated parameters in the initial set to guarantee homogeneity. In the end, points having not been grown are interpolated by the successfully estimated neighbours.

3.2.2 DHI Algorithm

In fact, DHI is an SFS algorithm to obtain the improved height image. We mainly follow Zheng and Chellappa's algorithm (1991). Their algorithm is a constrained optimization problem minimizing

$$\iint F(p,q,Z)\, dx\, dy, \tag{10}$$

where

$$\begin{aligned} F = {} & [R(p,q) - I(x,y)]^2 + \\ & [R_p(p,q) \cdot p_x + R_q(p,q) \cdot q_x - I_x(x,y)]^2 + \\ & [R_p(p,q) \cdot p_y + R_q(p,q) \cdot q_y - I_y(x,y)]^2 + \\ & \mu \cdot [(p - Z_x)^2 + (q - Z_y)^2]^2. \end{aligned} \tag{11}$$

In their algorithm, the intensity gradient constraint and the height gradient constraint are applied. Using the calculus of variations, minimization of Eq. 10 is equivalent to solving the Euler equations:

$$F_p - \frac{\partial}{\partial x}F_{p_x} - \frac{\partial}{\partial y}F_{p_y} = 0, \quad (12.1)$$

$$F_q - \frac{\partial}{\partial x}F_{q_x} - \frac{\partial}{\partial y}F_{q_y} = 0, \quad (12.2)$$

$$F_Z - \frac{\partial}{\partial x}F_{Z_x} - \frac{\partial}{\partial y}F_{Z_y} = 0. \quad (12.3)$$

The Euler equations were simplified by taking the Taylor series of the reflectance map and representing the height, gradient and their derivatives in discrete form. An iterative strategy was applied. In a new iterative scheme, the height and gradients were updated simultaneously. Our algorithm differs from that of Zheng and Chellappa in two points. One is that we use both the Lambertian and the Torrance-Sparrow photometric models instead of only using the Lambertian model. The other is that we use the analytical way to calculated R_p and R_q instead of using the numerical way. Zheng and Chellappa numerically calculated R_p and R_q as

$$R_p = R(p,q) - R(p+\Delta p, q), \quad (13.1)$$

$$R_q = R(p,q) - R(p,q+\Delta q), \quad (13.2)$$

where $\Delta p = \Delta q$ is a positive small constant. This is reasonable because they started their algorithm in the zero initial values of both height and gradient. As there is an approximate height image, therefore the approximate p and q images are available, too; in our case, we analytically calculate R_p and R_q. For the Lambertian model, we have

$$R_p = p\cdot(1+p^2+q^2)^{-3/2}\cdot(s_z - s_x\cdot p - s_y\cdot q) - s_x/(1+p^2+q^2)^{1/2}, \quad (14.1)$$

$$R_q = q\cdot(1+p^2+q^2)^{-3/2}\cdot(s_z - s_x\cdot p - s_y\cdot q) - s_y/(1+p^2+q^2)^{1/2}, \quad (14.2)$$

where s_x, s_y and s_z are three components of the source direction. For Torrance-Sparrow model, we have

$$R_p = -c_d/g_1\cdot(p\cdot g_3/g_2 + s_x) - 2\cdot c_s\cdot c_r^2\cdot\alpha\cdot g_4\cdot\exp(-c_r^2\cdot\alpha^2)/g_1\cdot(p\cdot g_5/g_2 + h_x), \quad (15.1)$$

$$R_q = -c_d/g_1\cdot(q\cdot g_3/g_2 + s_y) - 2\cdot c_s\cdot c_r^2\cdot\alpha\cdot g_4\cdot\exp(-c_r^2\cdot\alpha^2)/g_1\cdot(q\cdot g_5/g_2 + h_y), \quad (15.2)$$

with

$$g_1 = (1+p^2+q^2)^{1/2},$$
$$g_2 = 1+p^2+q^2,$$
$$g_3 = s_z - s_x\cdot p - s_y\cdot q,$$
$$g_4 = -1/\sqrt{1-(\mathbf{H}\cdot\mathbf{N})^2},$$
$$g_5 = h_z - h_x\cdot p - h_y\cdot q,$$

where h_x, h_y and h_z are three components of the vector $\mathbf{H}$ (see Eq. 7).

4. EXPERIMENTS AND CONCLUSION

We tested our de-shading system with two height images: a DTM of the Mars area CALYDON FOSSA (from University College London) and the Mozart height image (see Fig. 4 and Fig. 5). The associated brightness images were synthetically generated by using three simulating photometric parameter maps with respect to the diffuse coefficient (c_d-map), specula coefficient (c_s-map) and surface roughness coefficient (c_r-map). They are shown in Fig. 6, Fig. 7 and Fig. 8, respectively. The values in the upper-left, upper-right, lower-left and lower-right quarters are 0.25, 0.5, 0.75 and 1 in Fig. 6, respectively; 0.75, 0.5, 0.25 and 0 in Fig. 7, respectively; 5, 7, 3 and 0 in Fig. 8, respectively. For the Mars DTM, Fig. 12 shows the synthetic brightness image by using the Lambertian model and c_d-map, Fig. 18 using the Torrance-Sparrow model and c_d, c_s and c_r-maps. The direction of light source is 0° azimuth and 45° slant in both Fig. 12 and Fig. 18. For the Mozart height image, Fig. 29 shows the synthetic brightness image by using the Lambertian model and the c_d-map, Fig. 34 using the Torrance-Sparrow model and c_d, c_s and c_r-maps. The direction of light source is 135° azimuth and 45° slant in both Fig. 29 and Fig. 34. In order to simulate the lower precision DTM, we down-sampled the two height images every four rows and every four columns. Then bi-linearly interpolated the points between the samples. Fig. 9 and Fig. 26 show the lower precision height images with respect to Fig. 4 and Fig. 5. In order to show the effect of down-sampling, we shaded Fig. 9 and Fig. 26 by using the Lambertian model and a constant c_d value (see Fig. 10 and Fig. 27). As the plotting size of the image in this paper is reduced, the detail is difficult to be seen. We plot the middle parts of the original images (see Fig. 11 and Fig. 28) to show the details. The re-shaded images in the same parts are plotted, too (see Fig. 16, Fig. 24, Fig. 33 and Fig. 40).

The system correctly estimated the photometric model in every image, i.e., the Lambertian model in Fig. 12 and Fig. 29, the Torrance-Sparrow model in Fig. 18 and Fig. 34. Fig. 13--14 show the obtained c_d map and updated DTM after de-shading. Fig. 15 shows the re-shaded image by using the same light source, the obtained c_d map and the updated DTM. Fig. 17 shows the re-shading result by changing the light source to (135°, 45°). Fig. 19--22 show the obtained c_d, c_s and c_r maps and updated DTM after de-shading. Fig. 23--25 show the same results as Fig. 15--17 but with the Torrance-Sparrow model. Fig. 30--33 and Fig. 35--40 show the same results as Fig. 13--16 and Fig. 19--24 but in the Mozart image. It should be pointed out that all the plotted images are linearly stretched in grey level. Tab. 1 (for the Lambertian Model) and Tab. 2 (for the Torrance-Sparrow Model) give mean square errors between the estimated maps and the original simulating maps of the photometric parameters; the mean square errors between the re-shaded brightness images and the original synthetic brightness images. In Tab. 1 and Tab. 2, the column Sn means the number of rows and columns used in down-sampling to generate the lower resolution of height images. The mean square errors of the brightness is based on the normalized values.

The results show our de-shading system works in what we expected. The re-shaded images by using the estimated photometric models, its corresponding parameters and the improved height images are close to their original brightness images. But the errors are also obvious, specially in the Torrance-Sparrow model. This is because that inside and near highlight boundaries the solution is quite unstable, and outside such boundaries $\exp(-c_r^2\cdot\alpha^2)$ is too small to allow a meaningful solution for c_r. It seems we need to improve both the algorithms of estimating the reflectance properties and SFS to reduce the error and improve the results. This will be our forward research task.

	Mars image		Mozart image	
Sn	c_d-map	brightness	c_d-map	brightness
2	0.0025	0.0377	0.0025	0.0024
3	0.0043	0.0418	0.0022	0.0039
4	0.0105	0.0448	0.0016	0.0055

Tab.1 Mean square errors for the Lambertian Model.

	Mars image				Mozart image			
Sn	c_d-map	c_s-map	c_r-map	brightness	c_d-map	c_s-map	c_r-map	brightness
2	0.0121	0.0997	6.4647	0.0509	0.0451	0.0319	6.0216	0.0318
3	0.0149	0.0329	6.3290	0.0550	0.0398	0.0581	6.0016	0.0335
4	0.0134	0.0563	6.2307	0.0489	0.0432	0.0991	6.0239	0.0338

Tab. 2 Mean square errors for the Torrance-Sparrow Model

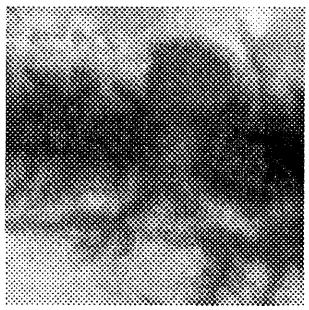

Fig. 4

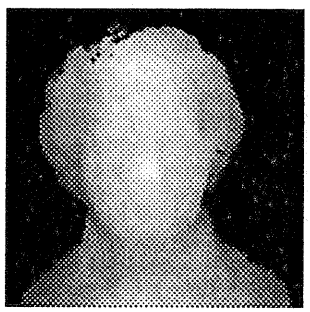

Fig 5

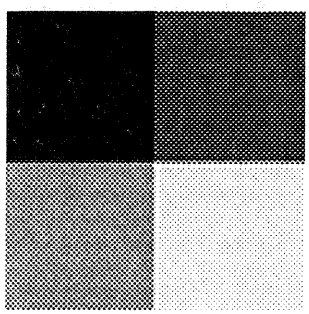

Fig. 6

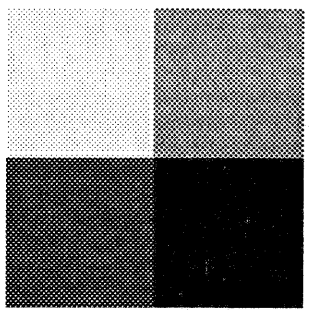

Fig.7

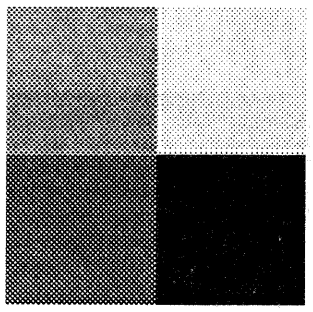

Fig. 8

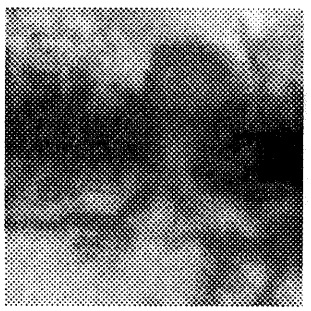

Fig. 9

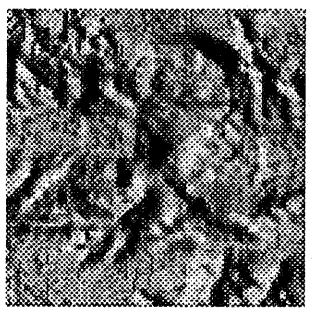

Fig. 10

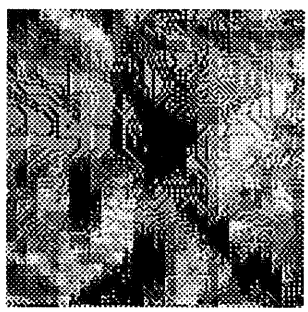

Fig. 11

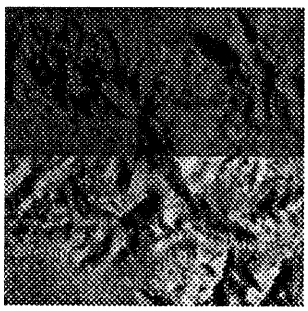

Fig. 12

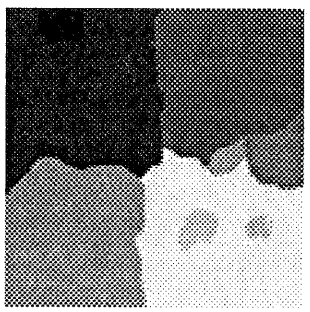

Fig. 13

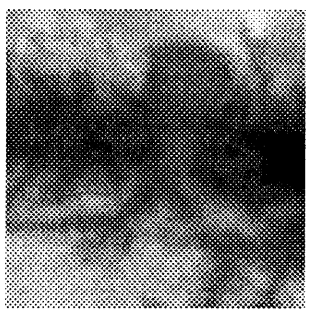

Fig. 14

Fig. 15

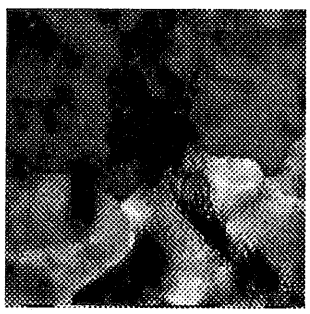

Fig. 16

Fig. 17

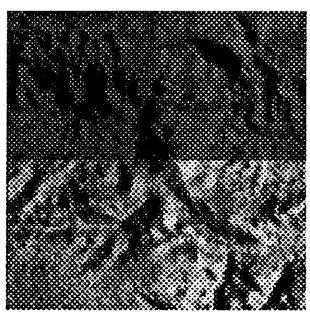

Fig. 18

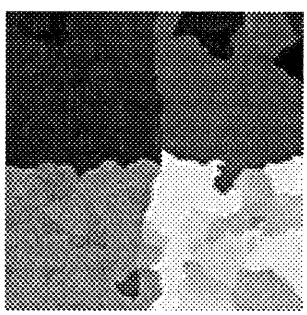

Fig. 19

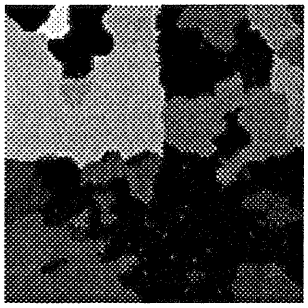

Fig. 20

Fig. 21

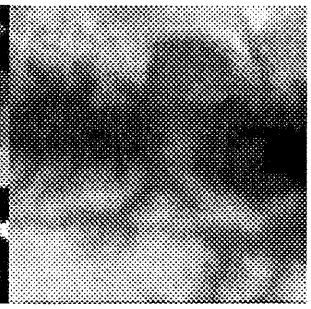

Fig. 22

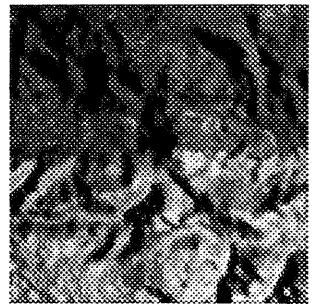

Fig. 23

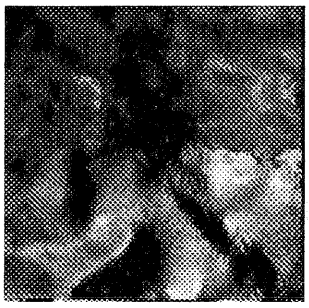

Fig. 24

Fig. 25

Fig. 26

Fig. 27

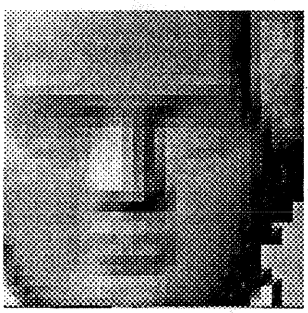

Fig. 28

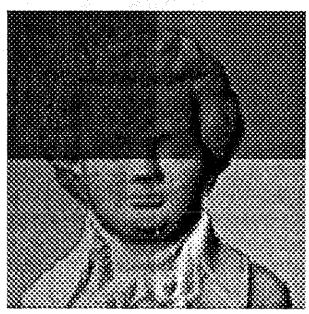

Fig. 29

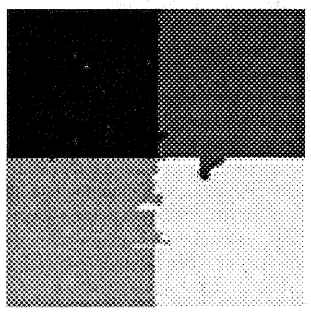

Fig. 30

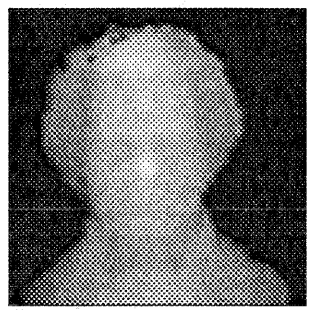

Fig. 31

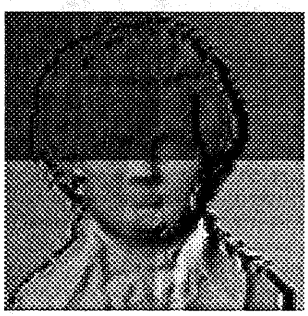

Fig. 32

Fig. 33

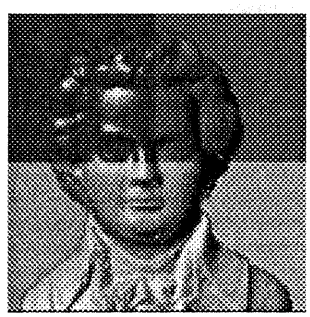

Fig. 34

Fig. 35

Fig. 36

Fig. 37

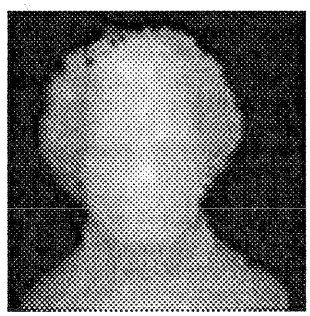

Fig. 38

Fig. 39

Fig. 40

Fig. 4 A DTM of the Mars area CALYDON FOSSA; Fig. 5 A Mozart height image; Fig. 6--8 Simulating c_d, c_s and c_r-maps; Fig. 9 Down-sampled image of Fig. 4; Fig. 10 Shaded image of Fig. 9; Fig. 11 The middle part of the original image of Fig. 10; Fig. 12 The synthetic brightness image by using the Lambertian model and c_d-map, the direction of light source is $0°$ azimuth and $45°$ slant; Fig. 13 The estimated c_d-map; Fig. 14 The improved DTM of Fig. 4; Fig. 15 The re-shaded image using the c_d-map in Fig. 13 and the same light source in Fig. 12; Fig. 16 The middle part of the original image of Fig. 15; Fig. 17 Same as in Fig. 15, but change the azimuth to be $135°$; Fig. 18 Same as in Fig. 12 but using the Torrance-Sparrow model; Fig. 19--21 The estimated c_d, c_s and c_r-maps; Fig. 22--25 Same as in Fig. 14--17 but with the Torrance-Sparrow model; Fig. 26--40 Same as in Fig. 9--25 but with Mozart image and without the re-shaded image by changing the azimuth.

REFERENCES

G. L. Bibro and W. E. Snyder, 1988. Fusion of range and reflectance image data using Markov random fields. In: Proc. IEEE International Symposium on Intelligent Control, Arlington, VA, pp. 154-158.

K. Brassel, 1974, A model for automated hill shading. The American Cartographer, 1(1), pp 15-27.

M. J. Brooks and B. K. P. Horn, 1985. Shape and source from shading. In: Proc. International Joint Conference on Artificial Intelligence, pp. 932-936.

B. K. P. Horn, 1982. Hill shading and the reflectance map. Geo-Processing, 2, pp 65-146,.

K. Ikeuchi and K. P. Horn, 1981. Numerical shape from shading and Occluding boundaries. Artificial Intelligence, 17(1-3), pp. 141-184.

K. Ikeuchi and K. Sato, 1991. Determining reflectance properties of an object using range and brightness images. IEEE Trans. on Pattern Analysis and Machine Intelligence, 13(11), pp. 1139-1153.

G. Kay and T. caelli, 1994. Inverting an illumination model from range and intensity map. CVGIP, 59(2), pp. 183-201.

R. Kimmel and A. M. Bruckstein, 1995. Global shape from shading. Computer Vision and Image Understanding, 62(3), pp. 360-369.

C. H. Lee and A. Rosenfeld, 1985. Improved methods of estimating shape from shading using the light source coordinate system. Artificial Intelligence, 26, pp. 125-143.

A. P. Pentland, 1982. Finding the illuminant direction. J. Opt. Soc. Amer. A, 72(4), pp. 448-455.

A. P. Pentland, 1984. Local shading analysis. IEEE Trans. on Pattern Analysis and Machine Intelligence, 6(2), pp. 170-187.

B. T. Phong, 1975. Illumination for computer generated pictures. Comm. of ACM, 18, pp. 311-317.

K. E. Torrance and E. M. Sparrow, 1967. Theory for off-specular reflection from roughened surface. J. Optical Society of America, 57 pp. 1105-1114.

Q. Zheng and R. Chellappa, 1991. Estimation of illuminant direction, albedo, and shape from shading. IEEE Trans. on PAMI, 13(7) pp. 680-702.

X. Zhou and E. Dorrer, 1995. An adaptive algorithm of shaded-relief images from DEMs based on wavelet transform. In: Proc. Digital Photogrammetry and Remote Sensing '95, St. Petersburg, Russia, SPIE series Vol. 2646, pp. 211-224.